Materials Science & Engineering A 876 (2023) 145165

Contents lists available at ScienceDirect

Materials Science & Engineering A

journal homepage: www.elsevier.com/locate/msea

Effects of notch-load-defect interactions on the local stress-strain fields and strain hardening of additively manufactured 18Ni300 steel

Shahriar Afkhami [a,c,*], Kalle Lipiäinen [a], Vahid Javaheri [b], Mohsen Amraei [c,d], Antti Salminen [d], Timo Björk [a]

[a] Laboratory of Steel Structures, LUT University, Lappeenranta, Finland
[b] Materials and Mechanical Engineering, University of Oulu, Oulu, Finland
[c] Laboratory of Laser Processing & Additive Manufacturing, LUT University, Lappeenranta, Finland
[d] Department of Mechanical and Materials Engineering, University of Turku, Turku, Finland

ARTICLE INFO

Keywords:
Additive manufacturing
Digital image correlation
Notch
Hardening
Steel
18Ni300

ABSTRACT

This study investigates the influence of geometrical notches on the local (true) stress-strain curves, deformations, and strain hardening behavior of maraging tool steel 18Ni300 processed via the laser powder-bed fusion method as an additive manufacturing approach. For this purpose, five types of specimens with different notch designs were manufactured; these samples were considered to study the effects of the notch stress concentration factor and the notch position on the material's mechanical response against the applied external load. Accordingly, using the digital image correlation technique, true stress-logarithmic strain curves were plotted and compared for various points in the vicinities of the notches while the specimens were subjected to quasi-static tensile loads. Further, the strain (work) hardening behavior of the material at each point was then evaluated and compared with other points by plotting their strain hardening diagrams from the first derivative of the stress-strain curves. The results showed that the strain hardening of the samples increased with the stress concentration factor (notch sharpness) while its ductility decreased accordingly. Furthermore, notch location and shape also showed determining roles in defining the material behavior. Ultimately, higher stress concentrations, internal positioning, and less gradual changes in geometric features (C-shaped notches compared to V-shaped ones) can result in higher defect sensitivity, more decrease in ductility, and more likely catastrophic failures in metals processed by additive manufacturing.

1. Introduction

Additive manufacturing (AM) has evolved during the past decades from a prototyping technique used primarily in laboratories to a manufacturing method commonly used nowadays in industrial fabrication units. AM owes its transition to its unique advantages and capabilities from its additive approach over conventional and subtractive fabrication methods. Additionally, AM can now process a wide variety of materials, from biomaterials to ceramics, polymers, and metals. Further, specifically in the case of metals, AM techniques such as laser powder bed fusion (L-PBF) can manufacture fully dense near net shape metallic components. As a result, these metallic parts can sometimes be used directly in their as-built form, without any further post-processing required, in various applications; however, in other cases, they might require some minor post-manufacturing procedures (e.g., light machining, polishing, and heat treatment) to become ready to service industrial products. In conclusion, compared to traditional manufacturing, methods like L-PBF have the potential to be used as a single-step building process or at least be a more sustainable replacement with lower material waste and shorter supply chains for subtractive manufacturing [1].

Design optimization and modification of metal parts are two other unique capabilities of AM, especially L-PBF, which are currently occasionally utilized in advanced high-performance metallic components used in critical applications such as aerospace, aeronautics, and automotive (e.g., Formula 1 cars) [2,3]. These components primarily utilize intricate internal and external geometric features to optimize performance while minimizing raw material consumption. This capability of L-PBF is of paramount importance as it can be utilized for components made of expensive metals (e.g., superalloys) used in harsh environments

* Corresponding author. Laboratory of Steel Structures, LUT University, Lappeenranta, Finland.
E-mail address: Shahriar.Afkhami@lut.fi (S. Afkhami).

https://doi.org/10.1016/j.msea.2023.145165
Received 30 March 2023; Received in revised form 8 May 2023; Accepted 15 May 2023
Available online 16 May 2023

(e.g., high temperatures or corrosive media); because it provides high strength-to-weight ratios and heat dissipation rates that are not possible with conventional manufacturing processes. However, such intricate geometries are typically accompanied by cross-sectional transitions, and these transitions, similar to notches, can act as stress risers and yield stress concentrations [4,5]. Furthermore, intense thermal gradients associated with additive manufacturing procedures such as L-PBF must be accounted for in addition to mentioned considerations. Metals exposed to such gradients can experience repetitive heating and cooling rates as high as 10^8 °K/s. Constant exposure to these rapid heating and cooling cycles can result in supersaturated or metastable microstructures, residual stress, porosity, lack of fusion, and micro-cracks in metals processed via L-PBF compared to their conventionally manufactured counterparts [3,6]. The interactions between these inhomogeneities and geometrical transitions in additively manufactured metals can yield outcomes different from what is generally expected in traditionally fabricated metals.

Accordingly, these issues are generally addressed in the newly developed and in-progress concept of "design for additive manufacturing" (DfAM) to avoid premature mechanical failures. However, metals processed by AM are commonly accompanied by flaws inherent to this manufacturing technology, e.g., porosity, lack of fusion, relatively rough surface quality, and residual stress. In other words, these inhomogeneities are inevitable in AM metal components, and their influence on the stress flow throughout the component must be considered while examining the effect of geometrical notches. For example, porosities and lack of fusions can act as local stress risers inside AM metals, while surface protrusions and valleys can act as external micro notches. Further, residual stresses based on their nature can increase or decrease the overall stress flow inside the component and alter its service life; in addition, interlayer boundaries as potential weak links can yield catastrophic failures. Acknowledging these issues becomes even more critical than usual when these inherent internal and external inhomogeneities cannot be remedied via post-fabrication treatments such as machining, polishing, heat treating, and hot isostatic pressing due to, for example, lack of accessibility of critical areas or cost-related difficulties [3,7–9].

Consequently, in such cases, the dominant competing features that determine the failure of AM metals are sudden cross-sectional changes associated with geometrical complexities acting as macro notches, local stress risers inherent in AM (like porosities), and the rough (as-built) surface features acting as micro notches. Consequently, numerous studies have investigated the simultaneous effects and interactions of notches and inhomogeneities in AM metals using typical experimental approaches such as quasi-static tensile and fatigue tests. However, these experiments provide insights into overall material behavior throughout a gauge area considered in standardized sample designs (e.g., engineering stress-strain curves), while the local response of the material to external loads remains unknown. Understanding this issue is essential since characteristics such as strain hardening influence metals' defect sensitivity, and an AM metal's defect sensitivity can be different along a geometrical notch root compared to the rest of the metal component [4,10,11].

Traditional load or displacement measurement tools such as extensometers and strain gauges are incapable of precise local measurements, and indeed they cannot provide simultaneous global and local (full-field) data during a mechanical test. However, newly developed inspection methods such as the digital image correlation (DIC) technique have made it possible to locally investigate the mechanical behavior of materials via directly measuring global and local deformations as a full-field data set. This technique carries out the measurements by sequential image registration and tracking; then, DIC systems can determine material deformations locally under a specific mechanical load increment by comparing two sequential images taken before and after that increment. Hence, thanks to DIC, it is now possible to calculate the true stress and logarithmic strain values of metal components beyond their necking limit. Consequently, it is also possible to locally study the hardening behavior of metals from point to point, e.g., along a notch root with significant stress concentration to the midplane of a bulk metal with plane stress condition [12,13].

Using traditional measurements, studies such as [14–18] investigated the effects of geometrical notches on the mechanical performance of AM metals. Further, studies such as [11,19–24], and [25] explored the simultaneous effects of geometrical (global) notches and flaws such as porosity, lack of fusion, and surface protrusions and valleys on the mechanical performance of AM metals. The mechanical performance in these studies was generally assessed in terms of engineering stress-strain curves and fatigue S–N diagrams. Following a similar route, the authors of the current work studied the simultaneous effects of various notches, AM inherent flaws, and external loads (notch-load-defect interactions) on the engineering stress-strain curve and fatigue life of 18Ni300 tool steel processed by L-PBF (hereafter abbreviated as L-PBF 18Ni300) [4]. However, the literature lacks research on the influence of such interactions on the local mechanical characteristics of metals and their hardening behavior, although such investigations are currently feasible thanks to techniques such as DIC, and their data can help researchers with making failure and fracture, e.g., finite element (FE), models more accurate. Consequently, the current study investigates the effects of notch-load-defect interactions on the mechanical behavior of 18Ni300 tool steel and probes its hardening behavior on a local scale. Ultimately, the results and discussion provided here shed more light on why AM metals, like the subject of this research, exhibit different levels of notch sensitivity compared to their conventionally manufactured counterparts.

2. Materials and methods

Fresh gas-atomized powder of tool steel 18Ni300 from EOS GmbH with a chemical composition presented in Table 1 was used as the raw material in this research. The samples were fabricated using an EOS M 290 machine equipped with a Yb-fibre laser with a 400 W maximum output; the utilized process parameters are presented in Table 2. Five different designs consisting of unnotched (UN), external sharp V-notch (ES), external blunt V-notch (EB), external blunt C-notch (EC), and internal sharp V-notch (IS) were considered in this research to investigate the effects of the shape, location, dimensions, and stress concentration factor of the notches on the stress-strain fields around their roots. The dimensions and geometrical characteristics of the specimens are presented in Fig. 1. All the samples were manufactured horizontally [building direction (BD) normal to the longitudinal axis] to avoid the occurrence of the staircase effect on the notch walls so that the mechanical behavior of the specimens could solely be attributed to the notch-load-defect interactions.

After AM of the specimens, their density was measured by the Archimedes method, and their defect distribution was analyzed using cross-sectional optical microscopy to ensure that the manufactured specimens were of acceptable quality; further information about the procedure is available in Ref. [4]. For the microstructural evaluations, $10 \times 10 \times 5$ mm^3 cubic specimens were ground and polished sequentially with abrasive pads and then were etched for 10 s with Nithal. After etching, high-magnification images were taken from the microstructure using a SU3500 scanning electron microscope (SEM). Regarding the samples prepared for the mechanical testing, the surface quality of the notched areas remained in their as-built condition to include the effect of raw surface features acting as micro notches in the study. The surface roughness values were measured by a KEYENCE VR-3200 3D microscope. Quasi-static tensile tests were carried out using a Galdabini Quasar 600 to evaluate the mechanical performance of the studied material. The tests were performed at 20 °C, under the constant strain rate of 10^{-3} s^{-1}, and were repeated once to ensure the reliability of the results.

An ARAMIS DIC system was used in conjunction with the tensile test

Table 1
Chemical composition of the raw powder according to its manufacturer [26].

Element	Ni	Co	Mo	Ti	Al	Cr	Cu	C	Mn	Si	P	S	Fe
wt%	17.00–19.00	8.50–9.50	4.50–5.20	0.60–0.80	≤0.15	≤0.50	≤0.50	≤0.03	≤0.10	≤0.10	≤0.01	≤0.01	Bal.

Table 2
L-PBF parameters used for manufacturing the samples.

Parameter	Laser power	Scanning rate	Hatch distance	Layer thickness	Scanning pattern
Value	200 W	1000 mm/s	70 μm	30 μm	meander

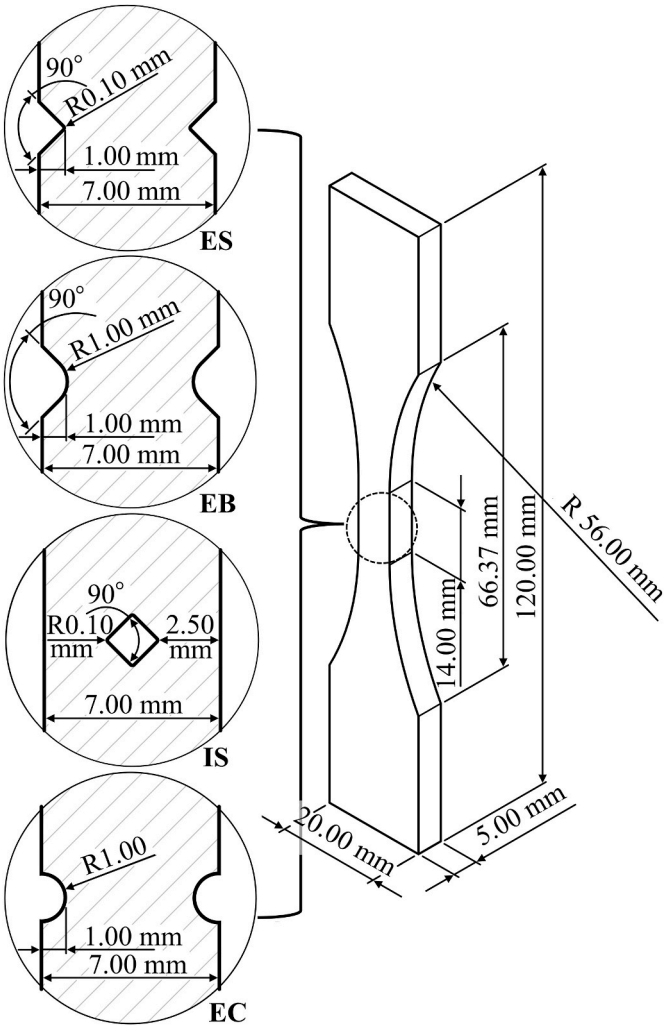

Fig. 1. Dimensions of the unnotched sample (right) and schematics of the notch designs for the notched specimens (left).

apparatus to measure the local strain values and plot the true stress-logarithmic strain curves. The GOM Correlate software (version 2019 Hotfix 7) calculated the true stress values via the Constant Volume approach by considering the actual true strain achieved from DIC, global external uniaxial load achieved from the load cell, and material continuity as the boundary condition. A deformation 12 M sensor was calibrated and used for the image recordings. For the calibration, the working distance, camera angle, and the distance between the cameras were 410 mm, 25°, and 142 mm, respectively, resulting in a calibration deviation of 0.036 pixels. Finally, FE models were developed to calculate the stress concentration factors of the notches, denoted as K_t in Table 3. These linear simulations were carried out using the FFEPlus solver from Dassault Systèmes. Tetrahedron elements ranging from 0.1 mm for the notch roots to 0.5 mm for the bulk material were employed to mesh the models. The model scale and mesh growth ratio were 1:1 and 1.1, respectively. As the boundary conditions, the modeled samples were fixed at one end to resemble the fixed grip of the actual test apparatus, while an external tensile load of 2000 N was applied on the other end to act as the moving grip of the test machine during the elastic deformation of the material. Also, a mesh convergence study was performed prior to the FE analyses to ensure the reliability of the models.

3. Results and discussion

Density measurements and analysis of defect contents revealed the material to be ≈ 99.9% dense with a density of ≈8.1 g/cm^3. Further, according to defect distribution data, most defects were of spheroidal nature (i.e., porosities) with a maximum diameter of ≈20 μm, uniform distributions, and no sign of clustering. Additionally, these sporadic porosities were accompanied by the rare presence of some lack of fusions, as marked by arrows in Fig. 2. By taking these results into account, the mechanical performance of the processed material was considered optimum in its as-built state, similar to specimens used in similar studies such as [4,27]. Regarding the microstructural features, according to the SEM images shown in Fig. 3, the microstructure of L-PBF 18Ni300 comprised a mixture of martensitic features with lath or cellular/dendritic morphologies (marked by A and B in Fig. 3, respectively). Also, sporadic islands of retained austenite were identified along the boundaries, as reported in Ref. [4]. Martensitic microstructures with such morphological features have been reported for similar maraging tool steels processed by L-PBF and are expected, considering the complex and intensive heating and cooling cycles associated with this technique [28–30]. Finally, the geometrical features of the notches according to their sample codes are summarized in Table 3 (further details on these data and their calculations are available in Ref. [4]).

3.1. Stress-strain fields around the external notches

Strain domains around the vicinities of the external notches (ES and EB in Fig. 1) are presented in Figs. 4 and 5 for the sharp and blunt notches, respectively. For the specimen with the sharp notches, a sequence of ten points starting from the notch root to the midplane of the specimen was selected for further investigation, as highlighted in Fig. 4. The true stress-logarithmic strain curves at these points are shown in Fig. 6. The curves in this figure contain the stress-strain data from the onset of the external loading until the final fracture of the specimen. The results showed that for a given external load (e.g., near the failure of the specimen ES), the resulting local true stress and plastic strain decreased

Table 3
Geometrical characteristics of the notches (further details are available in Ref. [4]).

Notch design	Root radius	Notch depth	Ra at the root	Rz at the root	Notch location	Calculated K_t
ES	0.1 mm	1.0 mm	5 μm	46 μm	External	6.3
EB	1.0 mm	1.0 mm	5 μm	50 μm	External	2.3
IS	0.1 mm	1.0 mm	–	–	Internal	6.6
EC	1.0 mm	1.0 mm	5 μm	50 μm	External	2.3

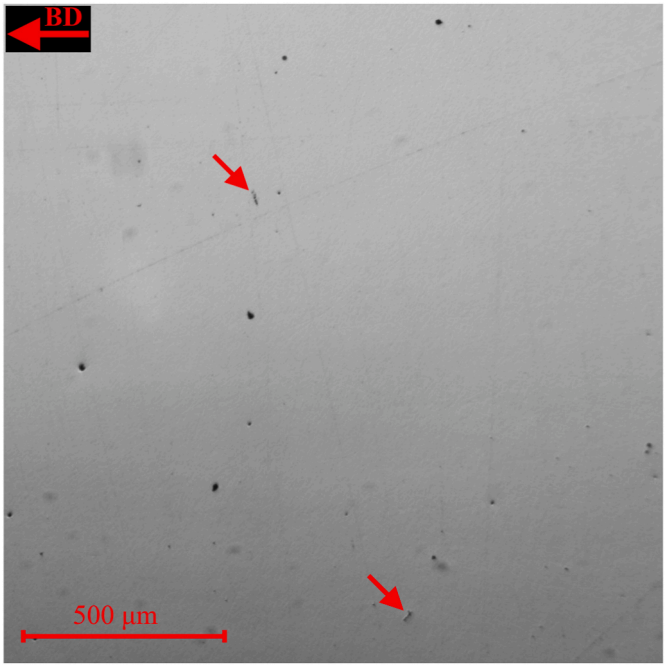

Fig. 2. Cross-sectional image from the unetched surface of L-PBF 18Ni300.

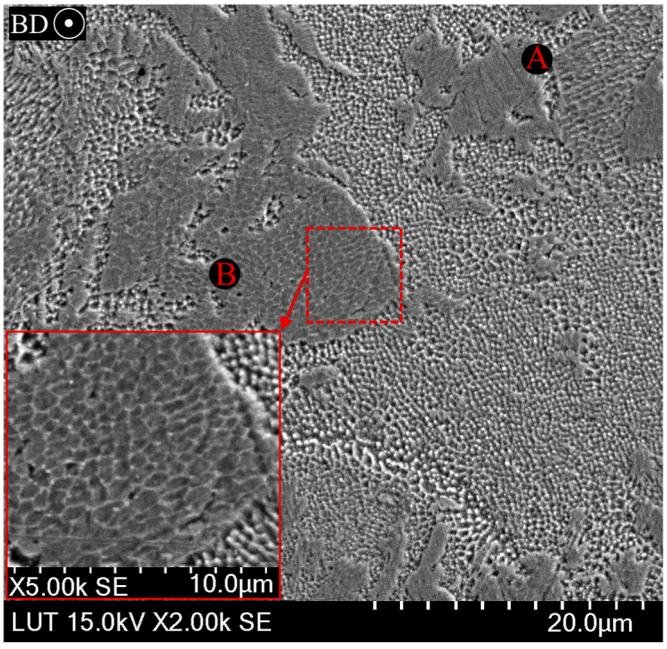

Fig. 3. Microstructural features of L-PBF 18Ni300 with cellular/dendritic subgrain structures shown in higher magnification. in the subset figure.

from the root to the midplane (see also Table 4), which agrees with the stress concentration expected in the notch vicinity. In addition, all points had lower elongation at break values than the unnotched specimen. Note that the negative slopes at the end of the curves for points 2–10 are due to the onset of failure at point 1 and its associated drop in force. Hence, these negative slopes were excluded from the analysis.

At first glance, under any given local stress (e.g., 1400 MPa in Table 5), the resultant logarithmic strain was higher near the notch root, showing an apparent softening behavior from the midplane to the notch root in Fig. 4, although the strain hardening curves (shown in Fig. 7) showed a more gradual decrease for dσ/dε near the notch root. This

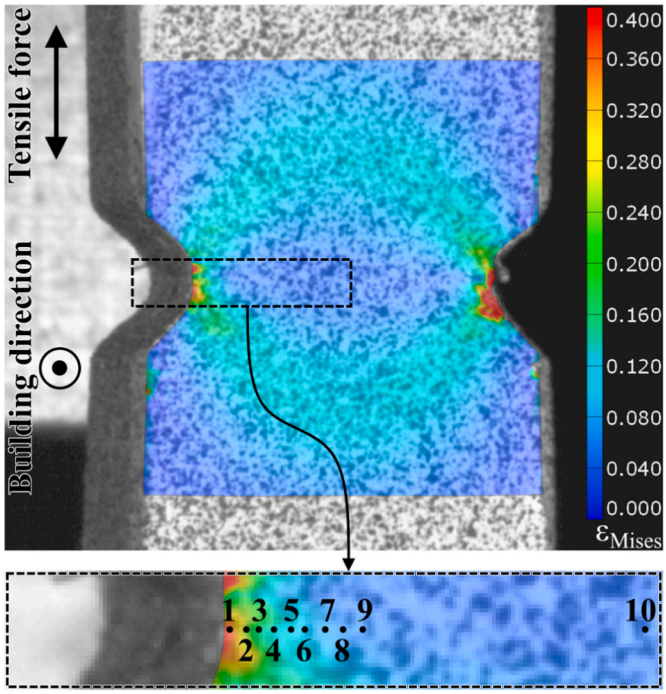

Fig. 4. Strain distribution data in the vicinity of the sharp notches in the ES specimen approximately prior to its final failure.

Table 4
Local stress and strain values at the external load of 26.8 kN for the ES sample.

Point	1	3	5	9
True stress	1400 MPa	1378 MPa	1361 MPa	1350 MPa
Logarithmic strain	0.0436	0.0270	0.0157	0.0074

Table 5
Global load and local strains at the local stress of 1400 MPa.

Point location in Fig. 4	**1**	3	5	9
Global external load	26.8 kN	27.1 kN	27.4 kN	27.6 kN
Logarithmic strain	0.0436	0.0329	0.0218	0.0137

contradiction can be attributed to the simultaneous influence of the stress triaxiality near the root and the more moderate boundary conditions acting on the material in this area compared to the midplane of the specimen (where the material is more constrained in each direction) [4]. In addition, the synergistic effects of the stress triaxiality attributed to the notch root and the stress multiaxiality resulting from the necking phenomenon may also exacerbate the issue regarding the controversial observation. Finally, the limitations of the calculation approach used for the true stress values at each point based on the constant volume (material continuity) should also be considered.

Therefore, to better evaluate the effects of notches on the hardening behavior of the material, the local stress-strain data of the two different notches were compared in Fig. 8. In this figure, for both notched samples (point 1 in Fig. 4 and point 1′ in Fig. 5), the diagrams are plotted from the onset of the external load until its value reaches the fracture limit of point 1 (final failure of the ES specimen). Therefore, all the parameters were set to be the same except for the notch design in this comparison. Consequently, point 1 in the root vicinity of the sharp notch experienced a higher stress concentration and triaxiality compared to point 1′ located in the root vicinity of the blunt notch.

According to Fig. 8, point 1 also experienced a higher level of strain hardening and a more moderate drop in dσ/dε values during its tensile

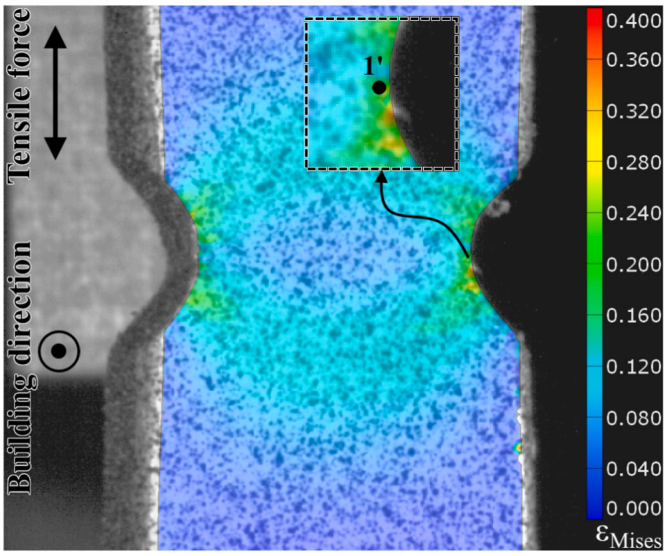

Fig. 5. Strain distribution data in the vicinity of the blunt notches in the EB specimen under the tensile load equal to the force value in Fig. 4.

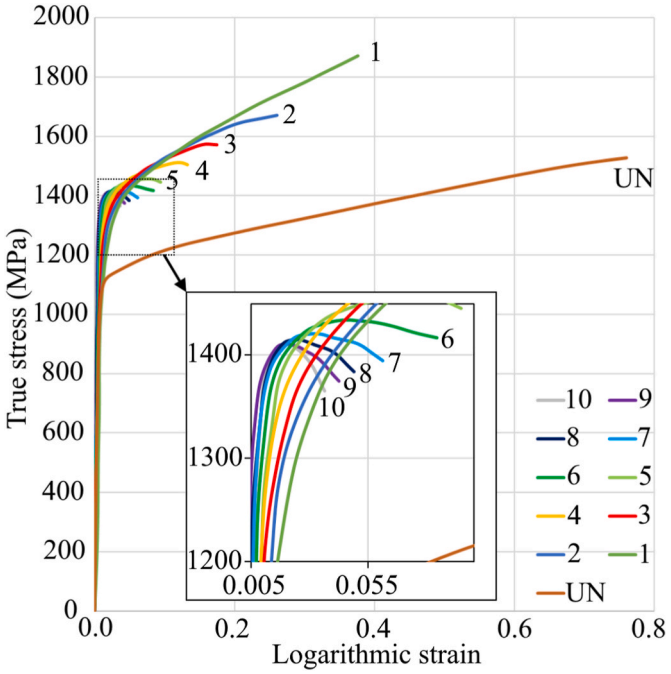

Fig. 6. True stress-logarithmic strain curves of the points shown in Fig. 4.

test. Thus, the existence of geometrical notches caused a more severe (local) strain hardening in the material, and the hardening increased with notch sharpness. In addition, the significantly lower ductility of the notched material compared to the unnotched sample can also be attributed to this phenomenon, making the material more defect sensitive in the notch vicinity. Finally, further fracture surface analysis of the broken sample with the blunt notch (see Ref. [4] for more details) also showed a higher level of microvoid coalescence mixed with brittle fracture along the notch root (compared to the midplane), which may also indicate the higher susceptibility to defects of the material near the notch root (Fig. 9, bottom right). As stated in Ref. [4], relatively higher microvoid coalescence in the notch vicinity can be attributed to the negative internal pressure caused by the stress triaxiality along the notch root; however, the limited presence of brittle fracture features remained

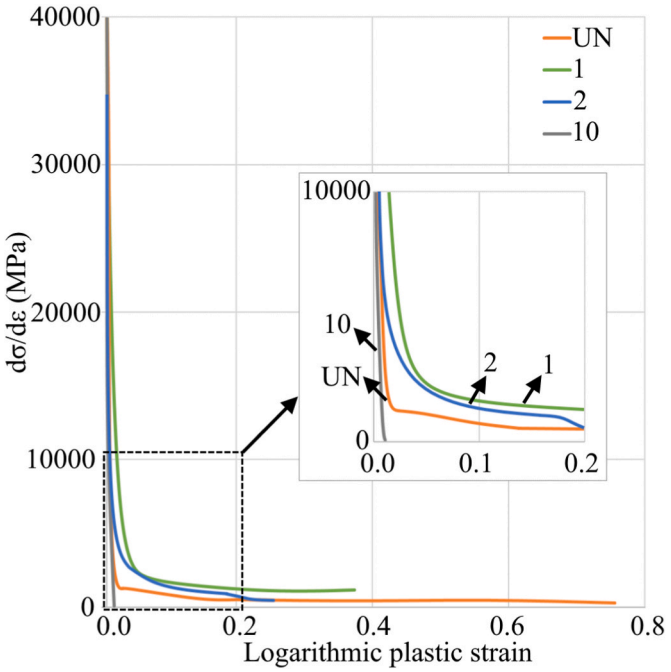

Fig. 7. Strain hardening curves of various points shown in Fig. 4 and their comparison to the strain hardening data from the unnotched sample.

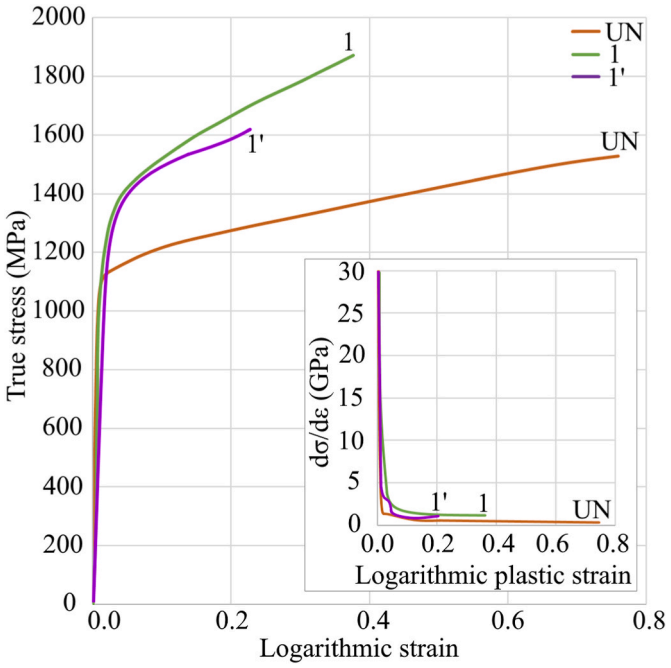

Fig. 8. True stress-logarithmic strain curves and strain hardening graphs of the points near the sharp (Fig. 4) and blunt (Fig. 5) notches, from the beginning of the tensile test until the external load of ≈26.8 kN.

unexplained solely relying on the stress state to analyze these features. Hence, these features can be linked to the different hardening behavior in the notch vicinity causing higher degrees of defect sensitivity and local brittleness.

3.2. *Influence of notch location*

Point 1″ in the IS specimen, with a distance from the root similar to that of point 1 in ES, was examined to study the influence of notch

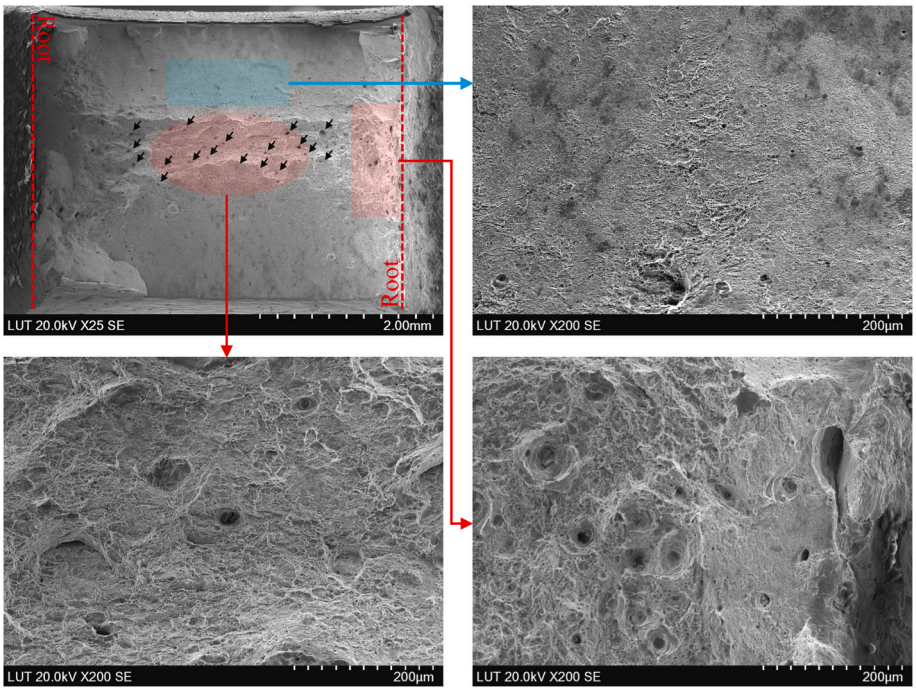

Fig. 9. Scanning electron microscopy of the fracture surface belonging to EB (from Ref. [4], used under CC BY 4.0 license).

location on the local stress-strain data in the root vicinity. As shown in Fig. 10, comparing the results from points 1 and 1″ showed that the stress concentration pattern of the internal and external notches matched through the elastic deformation of the material. However, under a fixed external load, material in the vicinity of the internal notch experienced lower levels of stress values during the plastic deformation, although both external and internal notches shared the same geometrical features and stress concentration factors. In addition, a higher drop rate of dσ/dε values for point 1″ also indicated a lower strain hardening capacity of the material in the root vicinity of the internal notches. Therefore, parameters other than the characteristics of geometrical notches must be the more determining factors ruling the plastic deformation of the material near the notch vicinity. Considering the possible influential factors in this regard, the material's boundary condition possibly causes the material to behave differently around the internal notch since it seems less constrained by its surroundings in the case of IS compared to ES, as qualitatively shown in Fig. 11. However, quantitative confirmation of this hypothesis requires further research. Further, material's interaction with inherent defects can be different in IS than in ES, as defect distribution in AM metals has been proven to be generally higher in subsurface areas, and the stress field in the case of IS is

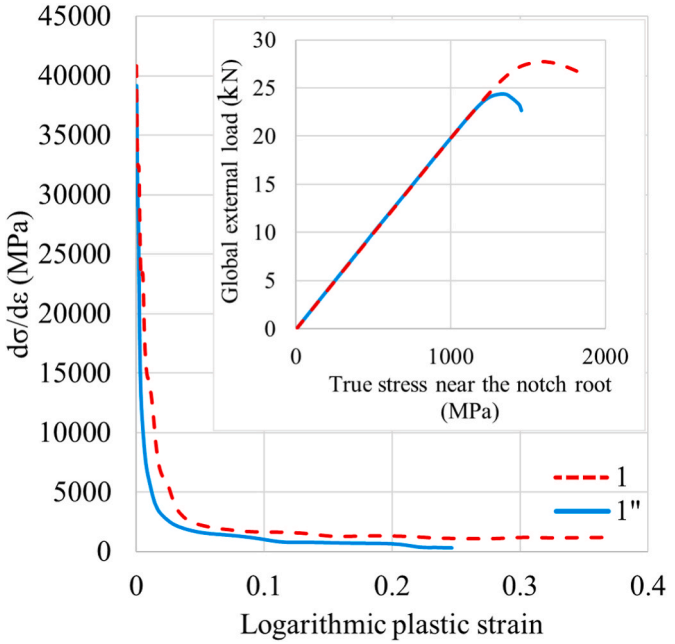

Fig. 10. Strain hardening curves and load-stress data (subset figure) of points 1 and 1″ in the samples ES and IS, respectively.

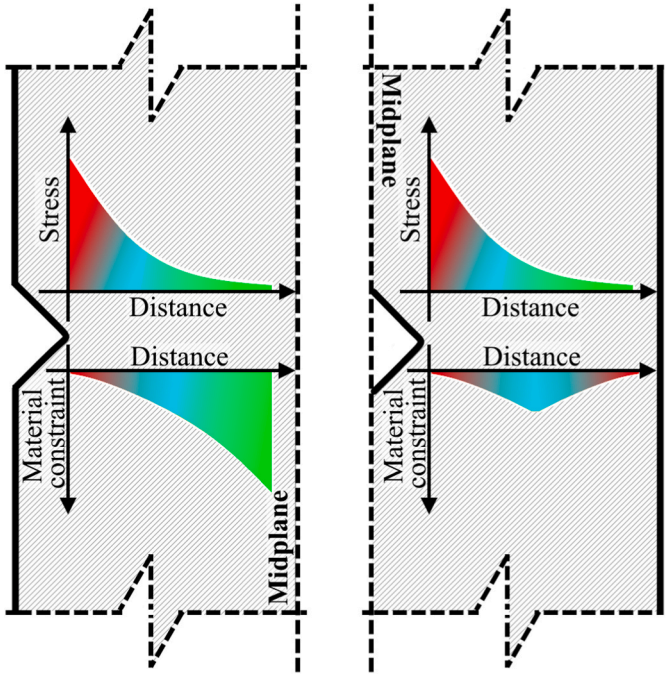

Fig. 11. Schematic view of the notches and variation of local stress and material's degree of restraint for ES (left) and IS (right) samples.

restricted between two subsurface areas (see Fig. 11) [31].

3.3. Influence of the global notch shape

Point 1‴ near the notch root of the EC specimen was examined and compared with point 1′ from the specimen EB to investigate the effects of the geometrical features of the notches on the stress-strain fields around the notch vicinity. These two notch designs were selected for comparison since they share similar geometrical features (radius and depth) and K_t values, but the notches in EC are semicircular, while EB has V-shaped notches, as shown in Fig. 1 and Table 3. The comparison showed that the two different notch designs imposed similar stress-strain values in the vicinity of their roots, as shown in Fig. 12. In conclusion, changing the notch shape from V-shaped to semicircular did not significantly alter the circumstances along the notch roots.

However, the ductility (elongation to failure) values of the samples, shown in the subset of Fig. 12, still showed a slightly different trend between EC and EB, regardless of the similarities discussed earlier. As shown in Fig. 13, in addition to stress-strain values around the notch vicinity, each notch design can also govern the strain rate of the material, especially along the notch root. Consequently, materials in the root vicinities of the notches in EC and EB specimens experienced different strain rates; this point is also true for the ES and IS samples. Furthermore, there is a consistency between the declining pattern of the ductility values in Fig. 12 and strain rates in Fig. 13. Deformation in strain rates relatively higher than quasi-static regimes can decrease the ductility of ferrous alloys [32,33]. Consequently, different ductility values from different notches with similar stress concentration factors, radii, and depths can be attributed to the various strain rates those notches impose on the material in their vicinities. The difference in the resultant strain rates from notches with similar K_t and dimensions can also be attributed to the boundary conditions and constraints applied to the material around the notch vicinities. However, further research is required in this regard.

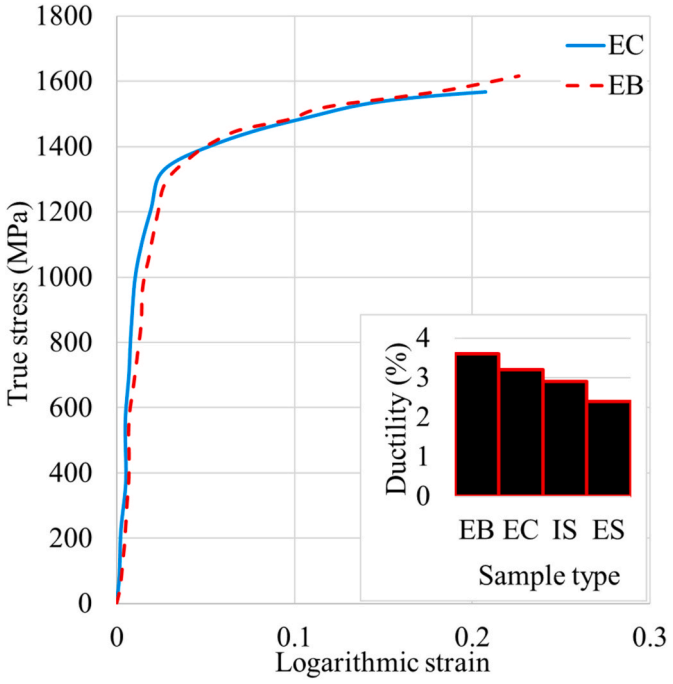

Fig. 12. Stress-strain data near the notch roots in the EB and EC specimens (points 1′ and 1‴, respectively) and ductility values of the specimens according to their notch designs (subset figure) [4].

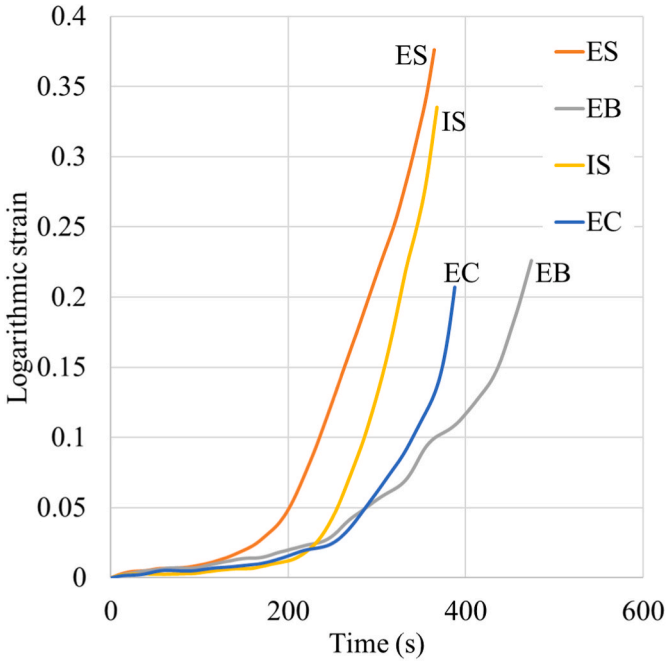

Fig. 13. Strain-time diagrams near the notch root of different specimens (points 1, 1′, 1″, and 1‴ from ES, EB, IV, and EC, respectively).

4. Conclusions

Five different notch designs were investigated in this research to evaluate the effect of notch designs and locations on the local stress-strain values in the specimens. These effects were discussed while considering the simultaneous influences of AM inherent defects and geometrical notches as global stress risers. Based on the results and their associated discussion, the following points can be highlighted as concluding remarks.

- The stress triaxiality (from the notches) and multiaxiality (from the necking) made the evaluation of the hardening behavior in the notch vicinity controversial. However, comparing the data from a sharp notch (with a relatively higher stress concentration factor and stress triaxiality) with a blunt notch yielded more conclusive results. The comparisons showed that the strain hardening of the material increased with the concentration factor (notch sharpness) while its ductility decreased accordingly.
- The changes mentioned above in the material behavior around the notch vicinities are expected to make the material more defect sensitive, which agrees with the observation from the previous study published in Ref. [4]. Furthermore, the higher sensitivity can exacerbate the negative influence of rough surface quality along the notch root. Hence, stricter safety measures and higher safety factors are expected to be applied on notched additively manufactured metals compared to their traditionally manufactured counterparts.
- Comparing an external notch with its internal peer with a similar shape and stress concentration factor showed that the external notch imposed higher strain hardening and stress concentration on the material, regardless of the geometrical similarities between the internal and external notches. Hence, the difference in the results achieved from these notches can be attributed mainly to the notch locations in the samples and possible constraints applied locally to the material by its surroundings. In other words, the material is expected to be more restrained by its surroundings inside the sample (e.g., near the midplane) than surface or subsurface areas.
- Comparing the notches with similar locations, dimensions, and characteristics but different shapes (semicircular vs. V-shaped)

showed that the material in the root vicinity of these notches experienced similar stress-strain fields. However, being under similar stress-strain domains does not guarantee the same response in such cases, as the sample with the semicircular notch showed lower overall ductility prior to its failure. Further investigation showed that the material experienced different strain rates in the case of these two notches, although the remaining parameters, even the stress-strain values, were similar in both cases. In this regard, the lower ductility can be attributed to the higher strain rate experienced by the material near the root vicinity of the semicircular notch.

Finally, further research to quantify these changes in material behavior in notch vicinities is recommended for future studies, as such analytical/numerical approaches can make the failure prediction of metals with geometrical notches processed by additive manufacturing more accurate. Also, future research seems essential, especially since the boundary condition and constraint degree of materials seem to be as determining as notch features, and similar or even identical notches can result in different failures based on their shapes or locations. In addition, the effect of material thickness is recommended to be considered for future studies since the majority of deductions and calculations made in this work, and numerous similar studies in the literature, are based on plane strain criteria. Therefore, understanding other extreme conditions, e.g., plane stress, and some middle grounds between such extremes, is required to comprehensively address how notches affect material behavior under different loading scenarios. However, even new techniques such as DIC cannot experimentally measure the stress-strain values through the thickness (inside materials); combinations of experimental and analytical approaches, such as simultaneous application of DIC and the finite element approach, might help to overcome such drawbacks. Furthermore, the influence of different loading types and directions, such as biaxial, multiaxial, or shear, also requires further research.

Originality statement

I write on behalf of myself and all co-authors to confirm that the results reported in the manuscript are original and neither the entire work, nor any of its parts have been previously published. The authors confirm that the article has not been submitted to peer review, nor has been accepted for publishing in another journal. The author(s) confirms that the research in their work is original, and that all the data given in the article are real and authentic. If necessary, the article can be recalled, and errors corrected.

CRediT authorship contribution statement

Shahriar Afkhami: Conceptualization, Methodology, Software, Investigation, Writing – original draft, Writing – review & editing, Visualization. **Kalle Lipiäinen:** Conceptualization, Methodology, Investigation, Validation. **Vahid Javaheri:** Methodology, Validation, Writing – review & editing. **Mohsen Amraei:** Methodology, Validation, Writing – review & editing. **Antti Salminen:** Writing – review & editing, Resources, Funding acquisition. **Timo Björk:** Writing – review & editing, Supervision, Resources, Methodology, Investigation, Funding acquisition, Conceptualization.

Declaration of competing interest

The authors declare that they have no known competing financial interests or personal relationships that could have appeared to influence the work reported in this paper.

Data availability

Data will be made available on request.

Acknowledgment

This study was carried out at LUT University as a part of the project DREAMS, funded by Business Finland. The authors would like to express their gratitude to all project partners. The help and support from Mr. Matti Koskimäki and Dr. Ilkka Poutiainen in managing the laboratory tests and procedures and Mr. Markus Korpela in manufacturing the specimens are highly appreciated. The authors also express special thanks for the technical support provided by the staff members at the laboratories of steel structures, laser materials processing, and additive manufacturing.

References

[1] Y. Zhang, L. Wu, X. Guo, S. Kane, Y. Deng, Y.G. Jung, J.H. Lee, J. Zhang, Additive manufacturing of metallic materials: a review, J. Mater. Eng. Perform. 27 (2018) 1–13, https://doi.org/10.1007/s11665-017-2747-y.
[2] The world's first 3D printed turbocharger | TD blog. https://www.turbodynamics.co.uk/media/blog/3d-printed-turbocharger, 2022. July 27.
[3] S. Afkhami, M. Dabiri, S.H. Alavi, T. Björk, A. Salminen, S. Habib Alavi, T. Björk, A. Salminen, Fatigue characteristics of steels manufactured by selective laser melting, Int. J. Fatig. 122 (2019) 72–83, https://doi.org/10.1016/j.ijfatigue.2018.12.029.
[4] S. Afkhami, E. Dabiri, K. Lipiäinen, H. Piili, T. Björk, Effects of notch-load interactions on the mechanical performance of 3D printed tool steel 18Ni300, Addit. Manuf. 47 (2021), 102260, https://doi.org/10.1016/J.ADDMA.2021.102260.
[5] E. Cyr, A. Lloyd, M. Mohammadi, Tension-compression asymmetry of additively manufactured Maraging steel, J. Manuf. Process. 35 (2018) 289–294, https://doi.org/10.1016/j.jmapro.2018.08.015.
[6] S. Afkhami, M. Dabiri, H. Piili, T. Björk, Effects of manufacturing parameters and mechanical post-processing on stainless steel 316L processed by laser powder bed fusion, Mater. Sci. Eng. 802 (2021), 140660, https://doi.org/10.1016/j.msea.2020.140660.
[7] S. Li, Y. Xin, Y. Yu, Y. Wang, Design for additive manufacturing from a force-flow perspective, Mater. Des. 204 (2021), 109664, https://doi.org/10.1016/J.MATDES.2021.109664.
[8] J. Plocher, A. Panesar, Review on design and structural optimisation in additive manufacturing: towards next-generation lightweight structures, Mater. Des. 183 (2019), 108164, https://doi.org/10.1016/J.MATDES.2019.108164.
[9] A. du Plessis, S.M.J. Razavi, M. Benedetti, S. Murchio, M. Leary, M. Watson, D. Bhate, F. Berto, Properties and applications of additively manufactured metallic cellular materials: a review, Prog. Mater. Sci. 125 (2022), 100918, https://doi.org/10.1016/J.PMATSCI.2021.100918.
[10] G. Nicoletto, R. Konečná, L. Kunz, M. Frkáň, Influence of as-built surface on fatigue strength and notch sensitivity of Ti6Al4V alloy produced by DMLS, MATEC Web of Conferences 165 (2018), 02002, https://doi.org/10.1051/matecconf/201816502002.
[11] K. Solberg, F. Berto, A diagram for capturing and predicting failure locations in notch geometries produced by additive manufacturing, Int. J. Fatig. 134 (2020), 105428, https://doi.org/10.1016/j.ijfatigue.2019.105428.
[12] G.M. Hassan, Deformation measurement in the presence of discontinuities with digital image correlation: a review, Opt Laser. Eng. 137 (2021), 106394, https://doi.org/10.1016/J.OPTLASENG.2020.106394.
[13] W. He, W. Shi, J. Li, H. Xie, In-situ monitoring and deformation characterization by optical techniques; part I: laser-aided direct metal deposition for additive manufacturing, Opt Laser. Eng. 122 (2019) 74–88, https://doi.org/10.1016/J.OPTLASENG.2019.05.020.
[14] S.M.J. Razavi, F. Berto, Fatigue strength of notched specimens made of Ti-6Al-4V produced by Selected Laser Melting technique, in: Procedia Structural Integrity, Elsevier B.V., 2018, pp. 74–78, https://doi.org/10.1016/j.prostr.2018.12.013.
[15] F. Brenne, T. Niendorf, Effect of notches on the deformation behavior and damage evolution of additively manufactured 316L specimens under uniaxial quasi-static and cyclic loading, Int. J. Fatig. 127 (2019) 175–189, https://doi.org/10.1016/j.ijfatigue.2019.05.018.
[16] K. Solberg, D. Wan, F. Berto, Fatigue assessment of as-built and heat-treated Inconel 718 specimens produced by additive manufacturing including notch effects, Fatig. Fract. Eng. Mater. Struct. 43 (2020) 2326–2336, https://doi.org/10.1111/ffe.13300.
[17] L.P. Borrego, J.A.M. Ferreira, J.D.M. Costa, C. Capela, J. De Jesus, A study of fatigue notch sensibility on titanium alloy TiAl6V4 parts manufactured by selective laser melting, in: Procedia Structural Integrity, Elsevier B.V., 2018, pp. 1000–1005, https://doi.org/10.1016/j.prostr.2018.12.186.
[18] S.-M.-J. Razavi, P. Ferro, F. Berto, Fatigue assessment of Ti–6Al–4V circular notched specimens produced by selective laser melting, Metals 7 (2017) 291, https://doi.org/10.3390/met7080291.
[19] S.M.J. Razavi, F. Berto, Directed energy deposition versus wrought Ti-6Al-4V: a comparison of microstructure, fatigue behavior, and notch sensitivity, Adv. Eng. Mater. 21 (2019), 1900220, https://doi.org/10.1002/adem.201900220.
[20] K. Solberg, F. Berto, Notch-defect interaction in additively manufactured Inconel 718, Int. J. Fatig. 122 (2019) 35–45, https://doi.org/10.1016/j.ijfatigue.2018.12.021.

[21] M. Benedetti, C. Santus, Building the Kitagawa-Takahashi diagram of flawed materials and components using an optimized V-notched cylindrical specimen, Eng. Fract. Mech. 224 (2020), 106810, https://doi.org/10.1016/j.engfracmech.2019.106810.
[22] G. Nicoletto, Directional and notch effects on the fatigue behavior of as-built DMLS Ti6Al4V, Int. J. Fatig. 106 (2018) 124–131, https://doi.org/10.1016/j.ijfatigue.2017.10.004.
[23] G. Nicoletto, R. Konečna, M. Frkan, E. Riva, Influence of layer-wise fabrication and surface orientation on the notch fatigue behavior of as-built additively manufactured Ti6Al4V, Int. J. Fatig. 134 (2020), 105483, https://doi.org/10.1016/j.ijfatigue.2020.105483.
[24] M. Kahlin, H. Ansell, J.J. Moverare, Fatigue behaviour of notched additive manufactured Ti6Al4V with as-built surfaces, Int. J. Fatig. 101 (2017) 51–60, https://doi.org/10.1016/j.ijfatigue.2017.04.009.
[25] M. Peron, J. Torgersen, P. Ferro, F. Berto, Fracture behaviour of notched as-built EBM parts: characterization and interplay between defects and notch strengthening behaviour, Theor. Appl. Fract. Mech. 98 (2018) 178–185, https://doi.org/10.1016/j.tafmec.2018.10.004.
[26] EOS GmbH, EOS MaragingSteel MS1, 2018. https://www.eos.info/en/additive-manufacturing/3d-printing-metal/dmls-metal-materials/tool-steel. (Accessed 25 April 2023). accessed.
[27] S.L. Campanelli, N. Contuzzi, A.D. Ludovico, Manufacturing of 18 Ni Marage 300 steel samples by selective laser melting, in: Adv Mat Res, Trans Tech Publications Ltd, 2010, pp. 850–857. https://doi.org/10.4028/www.scientific.net/AMR.83-86.850.
[28] P. Bajaj, A. Hariharan, A. Kini, P. Kürnsteiner, D. Raabe, E.A. Jägle, Steels in additive manufacturing: a review of their microstructure and properties, Mater. Sci. Eng. 772 (2020), 138633, https://doi.org/10.1016/j.msea.2019.138633.
[29] M. Sanjari, A. Hadadzadeh, A. Shahriairi, S. Tamimi, H. Pirgazi, B.S. Amirkhiz, L. Kestens, M. Mohammadi, On the effect of building direction on the microstructure and grain morphology of a selective laser melted maraging stainless steel, in: Minerals, Metals and Materials Series, Springer, 2020, pp. 285–295, https://doi.org/10.1007/978-3-030-36296-6_27.
[30] S. Afkhami, V. Javaheri, E. Dabiri, H. Piili, T. Björk, Effects of manufacturing parameters, heat treatment, and machining on the physical and mechanical properties of 13Cr10Ni1·7Mo2Al0·4Mn0·4Si steel processed by laser powder bed fusion, Mater. Sci. Eng., A 832 (2022), 142402, https://doi.org/10.1016/j.msea.2021.142402.
[31] N. Sanaei, A. Fatemi, N. Phan, Defect characteristics and analysis of their variability in metal L-PBF additive manufacturing, Mater. Des. 182 (2019), 108091, https://doi.org/10.1016/J.MATDES.2019.108091.
[32] M. Shahanur Hasan, D. De Pellegrin, R. Clegg, C. Yan, Johnson-Cook model parameters determination for 11% and 14% Mn-Steel, Mater. Sci. Eng., B 283 (2022), 115788, https://doi.org/10.1016/J.MSEB.2022.115788.
[33] J.A. Lichtenfeld, M.C. Mataya, C.J. Van Tyne, Effect of strain rate on stress-strain behavior of alloy 309 and 304L austenitic stainless steel, Metall. Mater. Trans. 37 (37) (2006) 147–161, https://doi.org/10.1007/s11661-006-0160-5.